Title

Inactivation of a Gα(s)-PKA tumour suppressor pathway in skin stem cells initiates basal-cell carcinogenesis.

Journal

Nature Cell Biology, 17(6)

Authors

Iglesias-Bartolome, Ramiro

Torres, Daniela

Marone, Romina

et al.

Publication Date

2015-06-01

DOI

10.1038/ncb3164

Peer reviewed

Published in final edited form as:

Nat Cell Biol. 2015 June ; 17(6): 793–803. doi:10.1038/ncb3164.

Inactivation of a Gαs-PKA tumor suppressor pathway in skin stem cells initiates basal-cell carcinogenesis

Ramiro Iglesias-Bartolome[1], **Daniela Torres**[1,5], **Romina Marone**[1,5], **Xiaodong Feng**[1], **Daniel Martin**[1], **May Simaan**[1], **Min Chen**[2], **Lee S. Weinstein**[2], **Susan S. Taylor**[3,4], **Alfredo A. Molinolo**[1], and **J. Silvio Gutkind**[1,6]

[1]Oral and Pharyngeal Cancer Branch, National Institute of Dental and Craniofacial Research, National Institutes of Health, Bethesda, Maryland 20892, USA

[2]National Institute of Diabetes and Digestive and Kidney Diseases, National Institutes of Health, Bethesda, Maryland 20892, USA

[3]Department of Pharmacology, University of California San Diego, La Jolla, California 92093, USA

[4]Department of Chemistry and Biochemistry, University of California San Diego, La Jolla, California 92093, USA

Abstract

Genomic alterations in *GNAS*, the gene coding for the Gαs heterotrimeric G-protein, are associated with a large number human of diseases. Here, we explored the role of Gαs on stem cell fate decisions by using the mouse epidermis as a model system. Conditional epidermal deletion of *Gnas* or repression of PKA signaling caused a remarkable expansion of the stem cell compartment, resulting in rapid basal cell carcinoma formation. In contrast, inducible expression of active Gαs in the epidermis caused hair follicle stem cell exhaustion and hair loss. Mechanistically, we found that Gαs-PKA disruption promotes the cell autonomous Sonic Hedgehog pathway stimulation and Hippo signaling inhibition, resulting in the non-canonical activation of GLI and YAP1. Our study highlights an important tumor suppressive function of Gαs-PKA, limiting the proliferation of epithelial stem cells and maintaining proper hair follicle homeostasis. These findings can have broad implications in multiple pathophysiological conditions, including cancer.

[6]Correspondence should be addressed to: J.S.G (sg39v@nih.gov).
[5]These authors contributed equally to this work

AUTHOR CONTRIBUTIONS

R.I.B., D.T., R.M., X.F., D.M. and M.S. performed experimental work and data analysis. M.C. and L.S.W. provided *Gnas* Floxed animals. S.S.T. designed PKI and assisted with PKA related experiments. A.A.M. performed pathology analysis. R.I.B. and J.S.G. designed experiments and wrote manuscript.

COMPETING FINANCIAL INTERESTS

The authors declare no competing financial interests.

Accession numbers: The microarray data set is available in the GEO database. GEO accession: GSE58894.

Among the rapidly self-renewing tissues in the adult body, the epidermis is a unique system to study stem cell biology[1–5]. Its integrity is highly dependent on resident self-renewing stem cells located in the basal layer of the stratified epidermis. Stem cells have to balance self-renewal and differentiation to maintain proper tissue homeostasis and respond to a variety of conditions, including tissue injury. This proper balance is achieved in part by a milieu of micro-environmental signals controlling stem cell fate decisions and their cellular responses.

G-protein-coupled receptors (GPCRs) are the largest family of cell-surface molecules involved in signal transduction, which play central roles in numerous physiological processes and pathological conditions[6, 7]. However, our understanding of the functions of GPCRs and their linked heterotrimeric G-proteins in stem cell biology *in vivo* is still largely incomplete. Here, by focusing on the role of Gαs on stem cell fate using the epidermis as a model system, we demonstrate that this Gα-protein exerts a central role in coordinating self-renewal and differentiation in epithelial stem cells. Conditional epidermal deletion of *Gnas* or inactivation of protein kinase A (PKA) in mice were alone sufficient to cause an aberrant expansion of the stem cell compartment, resulting in the rapid formation of basal cell carcinoma-like lesions. In contrast, expression of active Gαs caused hair follicle stem cell exhaustion and hair loss. Mechanistically, Gαs and PKA disruption promoted the concomitant cell autonomous activation of GLI and YAP1. These findings support a central role of Gαs and PKA in stem cell fate decisions in mammals, and reveal a tumor suppressive mechanism by which the Gαs-PKA signaling axis limits the aberrant proliferation of epithelial stem cells and maintains hair follicle and skin homeostasis.

RESULTS

Gnas deletion in the skin is sufficient to induce basal cell carcinoma-like lesions

To explore the role of Gαs on stem cell fate we generated epidermal-specific *Gnas* knockout mice. Mice expressing a tamoxifen-inducible Cre driven by the keratin 14 promoter (K14CreER), which targets the epidermal stem cell compartment[8], were crossed with mice carrying loxP sites surrounding *Gnas* exon one[9] (Fig. 1a). Unexpectedly, all *Gnas* epidermal knock-out mice (*Gnas* eKO) developed skin lesions characterized by thickening of the epidermis and hair loss, primarily on ears, snout and paws, only few weeks after *Gnas* excision (Fig. 1b–c, and Supplementary Fig. 1). Histologically, these lesions displayed extensive proliferation of basaloid cells, which formed clumps and islands that deeply invaded the underlying stroma (Fig. 1d). Tumors were morphologically similar to superficial and nodular human basal cell carcinomas (BCC)[10] (Fig. 1e), developing in body regions aligned with previous BCC mouse models[11, 12].

The epidermal basal identity of tumor lesions in *Gnas* eKO mice was confirmed by the expression of the basal marker cytokeratin 5 (CK5) and stem cell marker p63 (Fig 1f). Cells showed altered proliferation patterns and polarity, as reflected by Ki67 (Fig 1g) and integrin α6 staining, respectively (Fig. 1h), and were positive for the hair follicle and BCC marker cytokeratin 15 (CK15)[13] (Fig. 1i) but negative for the differentiation marker loricrin (Fig. 1j). Increased thickness of the CK15+ skin layer (Supplementary Fig. 1c) and multiple additional markers reflected the expansion of the basal cells. Thus, deletion of *Gnas* from

mouse epidermis is sufficient to induce rapid expansion of the stem cell compartment and development of lesions resembling BCC.

Transcriptional analysis in *Gnas* eKO mice uncovers the activation of Hedgehog GLI and Hippo YAP1 transcriptional networks

Gene ontology analysis of transcripts in the skin of *Gnas* eKO mice showed significantly increased expression of genes associated with epithelial development (Fig. 2a). Analysis of upregulated transcriptional signatures revealed alterations in multiple transcriptional networks (Supplementary Table 1) that were filtered by focusing on transcription factors with known functions in hair follicle and epidermal stem cell maintenance. These included GLI1, NFAT family genes, TP63, EZH2 and YAP1 (Fig. 2b). Interestingly, GLI transcription factors are the main drivers of human BCC development[3, 10, 11, 14]. We confirmed the overactivation of the GLI transcriptional network by analyzing the mRNA levels of Hedgehog signaling members in *Gnas* eKO mice (Fig. 2c–d). While GLI members and their transcriptional targets *Patch1* and *Patch2* were all upregulated, we did not detect increased mRNA levels of Sonic Hedgehog (*Shh)* or Indian Hedgehog (*Ihh)* (Fig. 2c). This might indicate that the stimulation of GLI signaling in *Gnas* eKO mice is cell autonomous, and does not depend on the increased expression of these PATCH ligands.

Lesions in *Gnas* eKO mice appeared to originate from hair follicles, raising the possibility that BCC development might be due to an amplification of a subset of hair follicle stem cells. Indeed, several transcriptional regulators of hair follicle stem cell maintenance and proliferation[12] were upregulated in *Gnas* eKO mice (Fig. 2e). Interestingly, GLI transcription factors are essential for hair follicle stem cell regeneration[3, 15] and the Hedgehog response gene *Gli1* defines a subset of stem cells that can regenerate the hair follicle and migrate into skin wounds during healing[16]. To track $GLI1^+$ cells after *Gnas* deletion we took advantage of GLI reporter mice (Gli^{lz})[17]. As previously described[2, 16], in *Gnas* wild type (WT) Gli^{lz} mice GLI1 is expressed almost exclusively in the isthmus and secondary hair germ of resting hair follicles (Fig. 2f–g). After *Gnas* deletion, however, $GLI1^+$ cells expanded to the entire hair follicle and spread to the interfollicular epidermis (Fig. 2g). In advanced lesions, most of the epidermis was replaced by $GLI1^+$ cells (Fig. 2g). These results confirmed the overactivation of the Hedgehog GLI signaling network following *Gnas* deletion, and suggested that BCC-like lesions might arise from an expansion of GLI^+ hair follicle stem cells.

In search for additional mechanisms leading to the massive hair follicle stem cell expansion after *Gnas* deletion, we next focused on YAP1, a transcriptional co-activator that maintains the self-renewal capacity and undifferentiated state of epidermal skin progenitor cells[18]. Recent reports indicate that YAP1 activity is tightly regulated by GPCRs[19]. Indeed, YAP1 transcriptional activity was significantly increased in *Gnas* eKO mice (Fig. 2b), concomitant with increased YAP1 nuclear localization (Fig. 2h–i). Additionally, a YAP1 transcriptional signature differentiated mRNAs from *Gnas* eKO mice from control mice by unsupervised hierarchical clustering (Fig. 2j). This approach helped identify multiple YAP1 targets that were significantly upregulated in *Gnas* eKO skin (Supplementary table 2). Human BCC also shows a significant increase in nuclear YAP1 throughout the tumor lesion (Fig. 2k–l).

Together, these results suggest that YAP1 activity in the epidermis might be tightly regulated by Gαs, and that YAP1 deregulation may contribute to BCC formation in mice and humans.

Gnas eKO triggers ectopic activation of GLI and YAP1

To further explore the role of GLI and YAP1 in stem cell expansion, we focused on early events triggered by *Gnas* deletion, before any phenotypic alterations were detected. Using whole mount of tail epidermis, we observed that shortly after *Gnas* excision (one day following tamoxifen treatment) GLI is ectopically activated in the base of the isthmus of hair follicles (Fig. 3a–b), while whole mount-immunofluorescence analysis revealed high nuclear localization of YAP1 in multiple areas within the base of hair follicles and interfollicular epidermis (Fig. 3c–d and Supplementary Fig. 2a). We confirmed the rapid increase in nuclear localization of YAP1 in ear skin sections (Supplementary Fig. 2b). These results provide evidence that increased YAP1 and GLI signaling precedes stem cell expansion and raise the possibility that YAP1 and GLI likely represent the drivers of BCC formation.

We next investigated the impact of *Gnas* deletion in epidermal cells by studying the repopulating capacity of individual epidermal stem cells *in vitro*[20, 21]. Cells isolated from the epidermis of *Gnas* eKO mice showed remarkably increased colony formation efficiency (Fig. 3e), confirming the expansion of the stem cell population. Furthermore, keratinocytes derived from *Gnas* eKO *Gli*^{lz} reporter mice showed increased LacZ+ colonies compared with WT cells and even WT cells treated with the Hedgehog signaling activator SAG[22] (Fig. 3f). To confirm the importance of GLI and YAP1 for the expansion of Gαs-depleted cells we performed RNA-interference experiments. Reduced expression of YAP1 or GLI1 resulted in a significant decrease colony forming efficiency of *Gnas* eKO cells (Fig. 3g). The broader impact of YAP1 knockdown might reflect the more extensive activation of YAP1 compared with GLI1 in *Gnas* eKO mice, or that other GLI transcription factors are involved in the proliferation of BCC cells. These results suggest that *Gnas* eKO triggers an ectopic and cell autonomous increase in GLI and YAP1 activity, which may contribute to aberrant epidermal stem cell proliferation.

Gαs restrains Hedgehog and YAP signaling through PKA

The absence of Gαs in the epidermis resulted in increased GLI and YAP1 signaling, suggesting that under normal conditions Gαs might limit the transcriptional activity of these stem cell regulators. Gαs controls a myriad of signaling networks, including cAMP signaling, cellular metabolism and intracellular trafficking[23, 24]. In search of the potential mechanisms underlying the impact of *Gnas* deletion we focused on the protein kinase-A (PKA), one of the main signaling effectors of Gαs downstream of cAMP activation[25]. To limit PKA activity, we took advantage of the PKA inhibitor protein (PKI)[26] and fused its PKA-interacting residues downstream of GFP (GFP-PKI) (Fig. 4a). Critical PKI residues were also mutated to disrupt binding to PKA (GFP-PKI4A) and used as a control (Fig. 4a). We also used a constitutively active mutant form of Gαs (GαsR201C[6]) or increased the intracellular levels of cAMP by combining forskolin and 3-isobutyl-1-methylxanthine

(IBMX) (FI), to confirm that GFP-PKI but not GFP-PKI4A blocks PKA signaling (Fig. 4b and Supplementary Fig. 2a–b).

These experimental tools demonstrated that the activation of PKA by Gαs exerts a remarkable negative impact on the transcriptional activity of GLI1 and YAP1 (Fig. 4c–d), the latter in line with recent reports[27, 28]. Furthermore, PKA could phosphorylate GLI1 (Fig 4e). This phosphorylation is known to regulate GLI transcriptional activity[29], suggesting that Gαs may control GLI directly through PKA, independently of Hedgehog signaling. Indeed, PKA inhibition by GFP-PKI was alone sufficient to significantly increase GLI1 transcriptional activity in 293 (Fig. 4c) and NIH-3T3 cells (Fig. 4f). This effect appears to be independent from the Hedgehog signaling protein smoothened (SMO), since GLI1 activation by GFP-PKI was only partially reduced by the SMO inhibitor cyclopamine (Fig. 4f).

To further explore this possibility we used keratinocytes derived from WT or *Gnas* eKO mice expressing the *Gli*^{lz} reporter. GLI transcriptional activity induced by SAG was abolished in *Gnas* WT *Gli*^{lz} keratinocytes by cyclopamine treatment (Fig. 4g–h). Instead, in *Gnas* eKO *Gli*^{lz} keratinocytes, GLI activity was only partially diminished by cyclopamine (Fig. 4g–h), while increasing the intracellular levels of cAMP had a stronger effect (Fig. 4g–h and Supplementary Fig. 4). Moreover, increased cAMP levels (but not cyclopamine) repressed the transcriptional activity of YAP1 in *Gnas* eKO keratinocytes, as judged by the levels of its transcriptional target *Ctgf* (Supplementary Fig. 4). Interestingly, deletion of *Gnas* also sensitized cells to Hedgehog pathway activation by SAG (Fig. 4g–h), supporting that *Gnas* acts as a Hedgehog-signaling restraining gene.

PKA mediates Gαs inactivation of YAP1 through LATS

YAP1 activity is mostly regulated post-transcriptionally through the inhibitory components of the Hippo pathway, which converge on the activation of LATS kinases that phosphorylate YAP1, inducing its cytoplasmic retention[30, 31]. Using a human keratinocyte cell line (HACAT) in which YAP1 is active under non-confluent conditions, stimulation of cAMP led to an increase in YAP1 phosphorylation and LATS1 activation, the latter revealed by its phosphorylation at the activation-loop (S909) (Fig. 5a). The induction of cAMP resulted in the phosphorylation of LKB1 and the Hippo core components MST1/2 (Fig. 5a), both of which have been shown to activate LATS and inhibit YAP1[30–32]. cAMP elevation also resulted in cytoplasmic retention of YAP1 in non-confluent cell cultures (Fig. 5b).

To investigate how PKA represses YAP1 activity, we used the cytoplasmic retention induced by cAMP as readout in RNA-interference experiments. Among the Hippo pathway components, only knockdown of LATS1/2 rescued the inhibitory effect of increased cAMP (Fig. 5c), suggesting that LATS kinases mediate PKA-induced YAP1 inhibition, at least in part independently of the core Hippo pathway components MST1/2 and SAV. Interestingly, LKB1 knockdown did not protect YAP1 from cAMP-mediated inhibition, while knockdown of the NF2 tumor suppressor partially rescued this effect (Fig. 5c). NF2 organizes Hippo signaling at the plasma membrane and coordinates the activation of LATS kinases and YAP1 phosphorylation[33]. Indeed, knockdown of LATS1/2 and NF2 abolished the cAMP-induced phosphorylation of YAP1, while knockdown of MST1/2, SAV and LKB1 had no

effect (Fig. 5d). NF2 knockdown also blocked the increased LATS1 phosphorylation induced by cAMP (Fig. 5d), supporting that NF2 contributes to the PKA-induced activation of LATS.

Inhibition of PKA in the skin is sufficient to phenocopy *Gnas* eKO

As PKA mediates the inhibitory effects of Gαs on GLI and YAP1, we next challenged the possibility that reduction in PKA activity might initiate BCC development. We generated mice expressing GFP-PKI and GFP-PKI4A under the control of the tet-responsive element and bred them with mice expressing the reverse tetracycline-activated transactivator rtTA2 under the control of the cytokeratin 5 promoter (K5rtTA), targeting the epidermis and its stem cell compartment[34, 35] (Fig. 6a).

When GFP-PKI (but not GFP-PKI4A) was expressed in the epithelium in response to doxycycline, mice rapidly developed extensive lesions in the skin, revealing histological features similar to human BCC that were indistinguishable from those of *Gnas* eKO mice (Fig. 6b–c). Skin and basal epithelial growths were positive for GFP (Fig. 6c), indicating the expression of GFP-PKI and GFP-PKI4A. Staining for CK5 and p63 confirmed the basal epithelial identity of these cells (Fig. 6d). Lesions were also positive for the hair follicle and BCC marker CK15 and showed altered proliferation patterns by Ki67 staining (Fig. 6e–f). Using *Gli*^{lz} reporter mice, we observed an expansion of GLI+ cells after GFP-PKI expression (Fig. 6g). Lesions were also positive for nuclear YAP1 (Fig. 6h). Furthermore, YAP1 was activated in K5rtTA tet-GFP-PKI keratinocytes, as measured by increased levels of YAP1 transcriptional targets *Ctgf* and *Cyr61*, and transcriptional regulators of hair follicle stem cell maintenance and proliferation (Fig. 6i).

Overactivation of Gαs induces epithelial stem cell differentiation and depletion

To investigate the impact of activating Gαs in the stem cell compartment, we next developed doxycycline-inducible mice expressing GαsR201C (tet-GαsR201C) and bred them with K5rtTA mice (Fig. 7a). GαsR201C expression was rapidly induced in keratinocytes derived from K5rtTA/tet-GαsR201C mice after doxycycline treatment (Fig. 7b). Remarkably, the persistent expression of active Gαs in mouse epidermis resulted in progressive hair loss (Fig. 7c) in both males and females. Hair follicles in K5rtTA/tet-GαsR201C mice terminally differentiated into keratinized cyst structures (Fig. 7d), suggesting that Gαs activation in the skin induces the nearly complete differentiation and exhaustion of hair follicle stem cells. Supporting this hypothesis, CD34+ hair follicle stem cells were depleted in K5rtTA/tet-GαsR201C mice (Fig. 7e). Gαs activation also led to a reduction in the basal progenitor markers p63 and CK5 (Fig. 7f) and decreased cell proliferation (Ki67 staining, Fig. 7g), particularly in the hair follicles. Furthermore, expression of GαsR201C resulted in a significant reduction in the colony forming efficiency of epidermal cells (Supplementary Fig. 5a–b). By using whole mount tail epidermis, we observed that GαsR201C induced the cytoplasmic retention of YAP1 and a decrease in the hair follicle stem cell marker CK15 (Fig. 7h and Supplementary Fig. 5c). Finally, cultured keratinocytes from K5rtTA/tet-GαsR201C mice showed increased expression of differentiation markers (Fig. 7i), and a concomitant reduction in hair follicle stem cell markers and GLI and YAP1 transcriptional activity (Fig. 7j). Collectively, these results

support the emerging concept that Gαs acts as a key regulator of epithelial stem cell fate in the skin.

Strikingly, the cyst formation observed on K5rtTA/tet-GαsR201C mice resembles the skin phenotype of mice were β-catenin is lost or repressed[36, 37]. However, by measuring the levels of *Axin2* mRNA, a well-known marker of β-catenin function, we could not find any differences in β-catenin pathway activation (not shown). One possible connection is that in β-catenin KO skin SHH signaling is lost[36]. Similarly, increased Gαs signaling blocks the transcriptional activity of GLI, suggesting that in both cases, suppression of Hedgehog signaling might result in hair follicle progenitor cells to lose their follicular differentiation and instead exhibit squamous epidermal characteristics, forming hair follicle-derived cysts[36]. Indeed, formation of epidermal-like cyst structures has been observed by conditional disruption of SHH signaling in the skin[38].

DISCUSSION

We demonstrate here that Gαs and PKA signaling function as non-canonical regulators of GLI and YAP1 transcriptional networks, controlling the proliferation and differentiation of epithelial stem cells and maintaining proper hair follicle and skin homeostasis (Fig. 8a).

PKA signaling can limit the activity of the Hedgehog pathway by a not fully understood mechanism[39–42]. Here we show that Gαs controls GLI activity directly through PKA, independently of SHH or SMO, and that repression of Gαs or PKA alone are sufficient to induce a cell autonomous increase on GLI-dependent transcription. We also present evidence that repression of Gαs or PKA results in the parallel activation of the YAP1 transcriptional network. Recent evidence indicates that PKA can block YAP1 through the activation of LATS kinases[27, 28]. Our experiments extend these prior findings, establishing that PKA mediates the inactivation of YAP1 downstream of Gαs through LATS by a mechanism that involves the NF2 tumor suppressor protein. In this regard, NF2 can be directly phosphorylated by PKA and this phosphorylation renders NF2 in an open conformation[43–45], known to be required for its interaction with LATS[33].

SHH and SMO signaling can increase YAP1 activity by upregulating its mRNA levels[46, 47]. However, we did not observe any increase in *Yap1* or *Shh* mRNAs upon Gαs or PKA inactivation and inhibition of SMO signaling by cyclopamine did not have any effect on the transcriptional activity of YAP1. On the other hand, YAP1 can induce expression of GLI1 mRNA[46], but YAP1 activation might not be sufficient to trigger Hedgehog signaling. Indeed, skin-specific knockout of Hippo signaling components resulting in increased YAP1 activity[33, 48–50] or overexpression of active mutants of YAP1[18, 51] do not result in the development of BCC-like lesions. Moreover, activation of GLI and YAP1 signaling occurs in both overlapping and distinct anatomical locations after *Gnas* deletion. Thus, while interplay between YAP1 and GLI may occur, the available information points towards the concomitant parallel activation of YAP1 and GLI, both initiated downstream from PKA inhibition (see Fig. 8). Of interest, although the evidence presented indicates that this activation of GLI and YAP1 might be the main cause of BCC development in our mouse models, several additional transcriptional networks were also upregulated after *Gnas*

excision (Supplementary Table 1). The elucidation of their precise intervening molecular mechanisms and potential cooperating roles in BCC development warrant further investigation.

Deregulation of the expression and activity of heterotrimeric G-proteins and GPCRs is frequently observed with human malignancies[6]. Activating mutations in *GNAS* promote aberrant growth of human thyroid[52] and pituitary tumors[53] and are found in multiple other neoplasms[6]. In contrast to its well-established tumor promoting role, our findings suggest that Gαs and its downstream effector PKA function as part of a tumor suppressive pathway in the skin. The disruption of this signaling axis is sufficient to promote rapid stem cell expansion and BCC formation, at least in part by relieving the restraining effect of Gαs and PKA on YAP1 and GLI (Fig. 8). These findings raise the possibility that Gαs and PKA might function as tumor suppressor genes in hyperproliferative diseases driven by GLI and YAP1 activation. In line with this, inactivating genomic alterations in *GNAS* have been found in SHH-driven medulloblastoma[42, 54], and ablation of *Gnas* in neural progenitors promotes medulloblastoma formation in mice with increased SHH signaling[42], suggesting that the tumor suppressive function of Gαs-PKA may have broad implications in multiple pathophysiological conditions.

Finally, GPCRs are essential for the maintenance of the epidermal stem cell compartment[3, 5]. Thus, we can postulate that Gαs and its yet to be defined coupled receptors may preserve the integrity and function of the epidermis and its resident self-renewing stem cells, ensuring proper tissue homeostasis and protecting from cancerous growth. We believe that this study will prompt the in depth analysis of alterations in Gαs and Gαs-coupled receptors, and perhaps Gαi-coupled receptors that counteract Gαs signaling, in future cancer genomic studies, in light of the unique stem cell regulatory and tumor suppressive functions of Gαs and PKA.

METHODS

DNA constructs

pCMX-Gal4-TEAD4 and pGL4.23-5×GAL4-binding UAS promoter luciferase have been described[55]. Human YAP1 was cloned by PCR from pDsRed Monomer C1-YAP2 (ADDGENE, Plasmid 19057) with a C-terminal FLAG tag into pCEFL (pCEFL FLAG-YAP1). Human GLI1 was cloned by PCR from pBluescript KS GLI K12 (ADDGENE, Plasmid 16419) with a C-terminal HA tag into pCEFL (pCEFL HA-GLI1) or with a C-terminal GAL4 DNA binding domain followed by HA tag into pCEFL (pCEFL GAL4HA-GLI1). The PKA inhibitor (PKI) was cloned by inserting the 24 amino acids after the initial methionine of the coding sequence of human PKI downstream of GFP (GFP-PKI). To use as a control, the phenylalanine and arginine residues of the PKI peptide were replaced to alanine to disrupt binding to PKA, named GFP-PKI4A (see Fig. 4a). *GNAS*R201C active mutant was generated using the Stratagene site directed mutagenesis approach and a Gαs long EE-tagged (internal) from Missouri S&T cDNA Resource Center (Catalog Number: GNA0SLEI00) as the wild type template.

Mice

All animal studies were carried out according to NIH-Intramural Animal Care and Use Committee (ACUC) approved protocols, in compliance with the Guide for the Care and Use of Laboratory Animals. Mice carrying a tamoxifen inducible Cre-mediated recombination system driven by the human keratin 14 promoter (K14CreER mice) were from The Jackson Laboratory [Stock Number 005107, STOCK Tg(KRT14-cre/ERT)20Efu/JK14Cre]. Epithelial-specific *Gnas* knockouts were obtained by crossing K14CreER mice with mice carrying loxP sites surrounding *Gnas* exon 1[56, 57]. *Gli*^{lz} reporter mice were already described[58] and they were obtained from The Jackson Laboratory [Stock Number: 008211, STOCK Gli1tm2Alj/J]. FVB/N mice carrying the cytokeratin 5 promoter in the reverse tetracycline transactivator (rtTA) (K5-rtTA) have been previously described[59]. For the generation of tet- GFP-PKI, tet- GFP-PKI4A and Tet-GαsR201C transgenic mice, the GFP-PKI, GFP-PKI4A and GαsR201C coding sequences were cloned downstream of the seven tet-responsive element (tetO7) in a modified pBSRV vector[60]. The fragment containing the expression cassette was isolated by PmeI digestion from vector DNA and purified for microinjection into FVB/N mice fertilized oocytes. Founders were identified for the presence of the transgene by screening genomic DNA from tail biopsies using a PCR reaction. The presence of wild-type, floxed and recombined Gsα was analyzed as previously described[57] The presence of the GFP-PKI and GFP-PKI4A transgenes was determined with the following primers: forward sequence 5′ CTAGAATTCGCTGTCTGCGA 3′, reverse sequence 5′ CTCGGCATGGACGAGCTGTA 3′, band approximately 1100 bp. The presence of the GαsR201C transgene was determined with the following primers: forward sequence 5′ CTAGAATTCGCTGTCTGCGA 3′, reverse sequence 5′ GCACTTTGGTTGCCTTCTC 3′, band approximately 620 bp. PCR reactions were performed with the following cycles: 95°C for 4 min, followed by 30 cycles of 95°C for 1 min, 55°C for 1 min, and 72°C for 1.5 min, and a final cycle with 10 min of extension at 72°C. The investigators were not blinded to allocation of samples during experiments and outcome assessment. Both male and female mice were used in the studies. Treatment was started between weeks 6 to 10 after birth. No statistical method was used to predetermine sample size. No randomization was used and all experiments were conducted using littermate controls. Doxycycline was administered in the food grain-based pellets (Bio-Serv) at 6g kg-1. Tamoxifen (1mg per mouse, per day, in corn oil) was applied by gavage to one month old mice for 5 consecutive days to induce homozygous deletion.

Cell lines, keratinocyte cell culture and transfections

All cells were cultured at 37°C in the presence of 5% CO2. HEK293, HACAT and NIH3T3 were obtained from ATCC and cells were cultured in DMEM (Invitrogen) containing 10% fetal bovine serum (FBS) (Sigma-Aldrich Inc) and antibiotic/antimycotic solution (Sigma-Aldrich Inc). Cells were transfected with Lipofectamine 3000 (Invitrogen) according to manufacturer's instructions. Keratinocytes from adult mice where isolated and cultured as previously described[61], except that defined keratinocyte serum free media (KSFM) (Invitrogen) supplemented with antibiotics was used as culture media. To assess colony-forming efficiency, equal number of cells from corresponding mice were plated in triplicate in six well plates and grown for 10 to 14 day and processed and quantified as previously

described[62]. Colonies were pseudo-colored red. For siRNA experiments, primary cells were transfected with the corresponding siRNAs two days after plating and HACAT cells were transfected one day after plating and in all cases cells were treated/harvested 48hs after transfection. siRNAs were: from Dharmacon siGENOME SMARTpool mouse Gli1 siRNA M-047917-01-0005, siGENOME SMARTpool mouse Yap1 siRNA M-046247-01-0005, ON-TARGETplus human NF2 siRNA L-003917-00-0005, ON-TARGETplus human SAV1 siRNA L-013070-01-0005, and non-targeting control siRNA D-001206-13; from IDT DsiRNA Duplexes human MST1 5′-AGUUGUCGCAAUUAAACA 5′-AGGUACUUGUUUAAUUGC, human MST2 5′-GCAGGUCAACUUACAGAU 5′-CCAUGGUAUCUGUAAGUU; from SIGMA MISSION siRNA human LATS2 SASI_Hs01_00158803, human LATS1 SASI_Hs01_00046128. siRNA was transfected at a concentration of 8 pmol cm-2 using Lipofectamine RNAiMAX (Invitrogen) according to manufacturer's instructions. β-Gal staining for cells was performed with the β-Gal Staining Kit (Invitrogen), except that staining was performed over a 48hs period in a wet chamber. β-Gal staining was visualized by confocal imaging[63]. Cyclopamine (InSolution™, Milipore) final 5 μM was added in 0.5% FBS DMEM for 24 hs for NIH3T3 cells and in supplement free-KSFM for 48hs for mouse keratinocytes. The smoothened agonist SAG (InSolution™, Milipore) final 100 nM was added to the media for 2 days before processing cells for β-Gal staining. Forskolin (Sigma) was used at 10 μM in combination with IBMX (Sigma) 100 μM in complete media for the indicated times.

Gene Expression Analysis and Quantitative PCR

Total skin and cultured keratinocytes RNA was isolated and processed using RNeasy Plus Mini Kit (Qiagen) according to manufacturer's instruction. Samples were excluded in cases were mRNA quality or tissue quality after processing was poor (bellow commonly accepted standards). Gene array analysis was performed with the Agilent Mouse GE 4×44K v2 Microarray Kit as previously described[64] using mRNA isolated from ear skin from four Gnas eKO mice with evident lesions (approximately 4 weeks after tamoxifen treatment) and four littermate controls. Gene Ontology (GO) terms were obtained with GeneSpringV10 by considering genes presenting a fold change greater or smaller than 1.8 or −1.8 respectively and GO terms were filtered for development terms. The functional analysis of transcriptional regulators was generated through the use of IPA (Ingenuity® Systems, www.ingenuity.com) using genes presenting a fold change greater than 1.8. YAP1 transcriptional signature was already described[55] and unsupervised clustering and expression levels were obtained using GeneSpringV10.

One microgram of cDNA was used as template for quantitative polymerase chain reaction with reverse transcription (qRT–PCR) analysis using iQ SYBR Green Supermix (Bio-Rad). Samples were analyzed using a Bio-Rad iCycler iQ multicolor real-time PCR detection system. Oligonucleotides used for amplification were (Gene, Forward sequence 5′→3′, Reverse sequence 5′→3′):

Rn18s GAAACTGCGAATGGCTCATTAAA
CCACAGTTATCCAAGTAGGAGAGGA

Gli1 TGGACAAGTGCAGGTAAAACC AATCCGGTGGAGTCAGACC

Gli2 GCAGACTGCACCAAGGAGTA CGTGGATGTGTTCATTGTTGA

Gli3 AACCCTATTCTACCCTCCAAA GCTGATAGTGCTGGTATTGCT

Ptch1 GGAAGGGGCAAAGCTACAGT TCCACCGTAAAGGAGGCTTA

Ptch2 CACCCCGCTTGACTGCTTCT GCCCACCTGTGCCTTATCTA

Lgr6 GGCTGGATGACAATGCACTCAC AGATTGTGCAGCCCCTCGAA

Lgr5 GCTCGGACCTGGGGCTCTCG TCTAGGCGCAGGGATTGAAGG

Sox9 TCGGTGAAGAACGGACAAGC TGAGATTGCCCAGAGTGCTCG

Tnc CAGGGATAGACTGCTCTGAGG CATTGTCCCATGCCAGATTT

Nfatc1 GGCGGGAAGAAGATGGTGCTGTC
TGGTTGCGGAAAGGTGGTATCTCA

Runx CTCCGTGCTACCCACTCACT ATGACGGTGACCAGAGTGC

Lhx2 ACGCTCGCAGGGCAGGGATAG AGTGCCCACGCCGTTGTAGTAGG

Yap1 CAGGAATTATTTCGGCAGGA CATCCTGCTCCAGTGTAGGC

Ctgf AGTCGCCTCTGCATGGTCA GCGATTTTAGGTGTCCGGAT

Krt10 GGAGGGTAAAATCAAGGAGTGGTA TCAATCTGCAGCAGCACGTT

Lor TCACTCATCTTCCCTGGTGCTT GTCTTTCCACAACCCACAGGA

Gnas GCAGAAGGACAAGCAGGTCT CCCTCTCCGTTAAACCCATT

Tail skin whole mounts and βGal stain

whole mounts where prepared and stained with antibodies (see below in Immunofluorescence) as previously described[65]. For βGal staining, back and ear skin were shaved in the area of dissection and skin was peeled off while cutting the attached subcutaneous layers. Skin and whole mounts were fixed in 2% paraformaldehyde, 0.2% glutaraldehyde, in PBS for 15′ on ice on each side. Then tissue was washed twice 20 min each with βGal wash solution (2 mM $MgCl_2$, 0.1% Nonidet P40, in PBS). Tissues were stained overnight at room temperature, in the dark, on a rolling platform in βGal stain solution [5 mM βgal stain: 10 mM $K_3Fe(CN)_6$, 10 mM $K_4Fe(CN)_6$.3H20, 2 mM $MgCl_2$, 0.1% Nonidet P40, 0.5 mg ml-1 X-gal in DMF, all diluted in PBS]. Afterwards, staining solution was removed and tissues were washed twice for 20 minutes each in βGal wash solution. Tissues were directly visualized or stored in ethanol 70% and processed for paraffin section and stained with Neutral Red or processed by cryosectioning.

Immunoblot Analysis

Western blot assays were performed as described previously[62, 66] and repeated at least 3 independent times. Antibodies used were: anti-GAPDH (Cell Signaling; clone no 14C10; catalogue no 2118; 1:2000), anti-α-Tubulin (Cell Signaling; clone no DM1A; catalogue no 3873; 1:2000), Phospho-PKA Substrate (RRXS*/T*) antibody (Cell Signaling; clone no 100G7E; catalogue no 9624; 1:1000), Phospho-(Ser/Thr) PKA Substrate Antibody (Cell

Signaling; catalogue no 9621; 1:1000), anti GFP (Covance; clone no B34; catalogue no MMS-118R; 1:1000), anti-HA tag antibody (Covance; clone no 16B12; catalogue no MMS-101R; 1:1000), anti-FLAG tag antibody (Sigma; clone no M2; catalogue no F3165; 1:1000), Glu-Glu (EE Tag; Covance; catalogue no MMS-115R; 1:1000), anti-Gαs (Millipore; clone no 385–394; catalogue no 371732; 1:1000), anti-phospho-PKA RII (pRSII; Millipore; catalogue no 04-404; 1:1000), YAP1 (Cell Signaling; clone no D8H1X; catalogue no 14074; 1:2000), Phospho-YAP Ser127 (Cell Signaling; catalogue no 4911; 1:1000), Phospho-YAP Ser397 (Cell Signaling; clone no D1E7Y; catalogue no 13619; 1:1000), LATS1 (Cell Signaling; clone no C66B5; catalogue no 3477; 1:1000), LATS2 (Bethyl Laboratories; catalogue no A300–479A; 1:500), Phospho-LATS1 Ser909 (Cell Signaling; catalogue no 9157; 1:1000), MST1 (Cell Signaling; catalogue no 3682; 1:1000), MST2 (Cell Signaling; catalogue no 3952; 1:500), Phospho-MST1 Thr183/MST2 Thr180 (Cell Signaling; catalogue no 3681; 1:500), LKB1 (Cell Signaling; clone no 27D10; catalogue no 3050; 1:1000), Phospho-LKB1 S428 (Cell Signaling; clone no C67A3; catalogue no 3482; 1:1000), SAV (Cell Signaling; clone no D6M6X; catalogue no 13301; 1:1000), NF2 (Cell Signaling; clone no D3S3W; catalogue no 12888; 1:1000), CREB1 (Santa Cruz; clone no C-21; catalogue no sc186; 1:100), Phospho-CREB Ser133 (Cell Signaling; clone no 87G3; catalogue no 9198; 1:500). Bands were detected using near-infrared fluorescence (Odyssey LI-COR Biotechnology) or Immobilon Western reagent (Millipore, MA) according to the manufacturer's instructions.

Luciferase Assays and Immunopurification

To measure YAP1 activity, cells in 12 or 24 well plates were co-transfected overnight with TEAD4-Gal4 (0.25 μg cm-2), UAS-luc (0.1 μg cm-2) plus the DNA constructs indicated in the figure: GFP (0.4 μg cm-2), YAP1 (0.2 μg cm-2), GαsR201C (0.2 μg cm-2), GFP-PKI (0.5 μg cm-2), GFP-PKI4A (0.5 μg cm-2). Next day cells were serum starved overnight and then luciferase activity was measured using a Dual-Glo Luciferase Assay Kit (Promega) and a Microtiter plate luminometer (Dynex Tech.). To measure GAL4-GLI1 activity, cells were co-transfected with GAL4-GLI1 (0.3 μg cm-2), UAS-luc (0.2 μg cm-2) plus the DNA constructs indicated in the figure at the same concentrations as for YAP1 activity and processed as indicated above. CRE assays were performed as described previously[67]. Luciferase normalization was performed in every case by co-transfecting a Renilla Luciferase Vector (0.025 μg cm-2) (Promega). Immunopurification was performed as previously described[62].

Immunofluorescence and Immunohistochemistry

Sections were processed and stained as previously described[62, 68]. Immunohistochemical analysis of YAP1 in human BCC was done on a tissue array (US Biomax BC21014). The following antibodies were used: mouse Ki-67 (Dako; clone no MIB-5; catalogue no M7249; 1:50), YAP1 (Cell Signaling; clone no D8H1X; catalogue no 14074; 1:500), p63 (Santa Cruz; clone no 4A4; catalogue no sc8431; 1:100), cytokeratin 5 (Covance; catalogue no PRB-160P; 1:500), cytokeratin 15 (Covance; catalogue no PCK-153P; 1:200), pan-cytokeratin (Dako; catalogue no Z0622; 1:500), loricrin (Covance; catalogue no PRB-145P; 1:500), integrin alpha6 (BD-PharMingen 555734; 1:200), GFP (Cell Signaling 2956; 1:200), anti-Mouse CD34 (eBoiscience 14-0341-85; 1:50). Nuclei were stained with Hoechst 33342

(Invitrogen). Tissue section images were taken with a Zeiss Axio Imager Z1 microscope equipped with an Apotome device (Carl Zeiss) using a Zeiss Plan APOCHROMAT 20x/0.8na objective and Zen 2012 software (Carl Zeiss). Whole mount fluorescent images were taken with a using an inverted Zeiss LSM 700 confocal microscope, coupled to Zen software 2010 (Carl Zeiss); 14–16 Z sections were taken with a Zeiss Plan APOCHROMAT 20x/0.8na objective and 3D maximum projections were made with Zen software 2010 (Carl Zeiss). Final images were bright contrast adjusted with Zen 2012 (Carl Zeiss) or PowerPoint. For histological analysis, tissues were embedded in paraffin; 3-μm sections were obtained and stained with H&E. Stained immunohistochemistry and H&E slides were scanned at 40× using an Aperio CS Scanscope (Aperio, CA, USA). Each immunostaining was repeated at least in 3 independent mice or 3 independent experiments and several fields were reviewed.

Statistical analysis

All analyses were performed in triplicate or greater and the means obtained were used for ANOVA or independent t-tests. Statistical analyses, variation estimation and validation of test assumptions were carried out using the Prism 5 statistical analysis program (GraphPad). Asterisks denote statistical significance (non-significant or NS, $P > 0.05$; *$P < 0.05$; **$P < 0.01$; and ***$P < 0.001$). All data are reported as mean ± standard error of the mean (s.e.m.).

Supplementary Material

Refer to Web version on PubMed Central for supplementary material.

Acknowledgments

This work was supported by the Intramural Research Program of the National Institutes of Health, National Institute of Dental and Craniofacial Research. R.M. was supported by grants from the Swiss National Science Foundation (Advanced Postdoc Mobility fellowship, SNF) and the Margarete und Walter Lichtenstein Stiftung. S.T. was supported by grant DK54441.

References

1. Blanpain C, Fuchs E. Epidermal homeostasis: a balancing act of stem cells in the skin. Nature reviews. Molecular cell biology. 2009; 10:207–217. [PubMed: 19209183]
2. Plikus MV, et al. Epithelial stem cells and implications for wound repair. Seminars in cell & developmental biology. 2012; 23:946–953. [PubMed: 23085626]
3. Arwert EN, Hoste E, Watt FM. Epithelial stem cells, wound healing and cancer. Nature reviews. Cancer. 2012; 12:170–180. [PubMed: 22362215]
4. Fuchs E, Chen T. A matter of life and death: self-renewal in stem cells. EMBO reports. 2013; 14:39–48. [PubMed: 23229591]
5. Barker N, Bartfeld S, Clevers H. Tissue-resident adult stem cell populations of rapidly self-renewing organs. Cell stem cell. 2010; 7:656–670. [PubMed: 21112561]
6. O'Hayre M, et al. The emerging mutational landscape of G proteins and G-protein-coupled receptors in cancer. Nature reviews. Cancer. 2013; 13:412–424.
7. Pierce KL, Premont RT, Lefkowitz RJ. Seven-transmembrane receptors. Nature reviews. Molecular cell biology. 2002; 3:639–650. [PubMed: 12209124]
8. Vasioukhin V, Degenstein L, Wise B, Fuchs E. The magical touch: genome targeting in epidermal stem cells induced by tamoxifen application to mouse skin. Proceedings of the National Academy of Sciences of the United States of America. 1999; 96:8551–8556. [PubMed: 10411913]

9. Chen M, et al. Increased glucose tolerance and reduced adiposity in the absence of fasting hypoglycemia in mice with liver-specific Gs alpha deficiency. J Clin Invest. 2005; 115:3217–3227. [PubMed: 16239968]
10. Crowson AN. Basal cell carcinoma: biology, morphology and clinical implications. Modern pathology : an official journal of the United States and Canadian Academy of Pathology, Inc. 2006; 19 (Suppl 2):S127–147.
11. Pasca di Magliano M, Hebrok M. Hedgehog signalling in cancer formation and maintenance. Nature reviews. Cancer. 2003; 3:903–911. [PubMed: 14737121]
12. Youssef KK, et al. Identification of the cell lineage at the origin of basal cell carcinoma. Nature cell biology. 2010; 12:299–305. [PubMed: 20154679]
13. Wang GY, Wang J, Mancianti ML, Epstein EH Jr. Basal cell carcinomas arise from hair follicle stem cells in Ptch1(+/−) mice. Cancer Cell. 2011; 19:114–124. [PubMed: 21215705]
14. Epstein EH. Basal cell carcinomas: attack of the hedgehog. Nature reviews. Cancer. 2008; 8:743–754. [PubMed: 18813320]
15. Hsu YC, Li L, Fuchs E. Transit-amplifying cells orchestrate stem cell activity and tissue regeneration. Cell. 2014; 157:935–949. [PubMed: 24813615]
16. Brownell I, Guevara E, Bai CB, Loomis CA, Joyner AL. Nerve-derived sonic hedgehog defines a niche for hair follicle stem cells capable of becoming epidermal stem cells. Cell stem cell. 2011; 8:552–565. [PubMed: 21549329]
17. Bai CB, Auerbach W, Lee JS, Stephen D, Joyner AL. Gli2, but not Gli1, is required for initial Shh signaling and ectopic activation of the Shh pathway. Development. 2002; 129:4753–4761. [PubMed: 12361967]
18. Zhang H, Pasolli HA, Fuchs E. Yes-associated protein (YAP) transcriptional coactivator functions in balancing growth and differentiation in skin. Proceedings of the National Academy of Sciences of the United States of America. 2011; 108:2270–2275. [PubMed: 21262812]
19. Yu FX, et al. Regulation of the Hippo-YAP pathway by G-protein-coupled receptor signaling. Cell. 2012; 150:780–791. [PubMed: 22863277]
20. Jensen KB, Driskell RR, Watt FM. Assaying proliferation and differentiation capacity of stem cells using disaggregated adult mouse epidermis. Nature protocols. 2010; 5:898–911. [PubMed: 20431535]
21. Franken NA, Rodermond HM, Stap J, Haveman J, van Bree C. Clonogenic assay of cells in vitro. Nature protocols. 2006; 1:2315–2319. [PubMed: 17406473]
22. Chen JK, Taipale J, Young KE, Maiti T, Beachy PA. Small molecule modulation of Smoothened activity. Proceedings of the National Academy of Sciences of the United States of America. 2002; 99:14071–14076. [PubMed: 12391318]
23. Dorsam RT, Gutkind JS. G-protein-coupled receptors and cancer. Nature reviews. Cancer. 2007; 7:79–94. [PubMed: 17251915]
24. Neves SR, Ram PT, Iyengar R. G protein pathways. Science. 2002; 296:1636–1639. [PubMed: 12040175]
25. Taylor SS, Ilouz R, Zhang P, Kornev AP. Assembly of allosteric macromolecular switches: lessons from PKA. Nature reviews. Molecular cell biology. 2012; 13:646–658. [PubMed: 22992589]
26. Knighton DR, et al. Structure of a peptide inhibitor bound to the catalytic subunit of cyclic adenosine monophosphate-dependent protein kinase. Science. 1991; 253:414–420. [PubMed: 1862343]
27. Kim M, et al. cAMP/PKA signalling reinforces the LATS-YAP pathway to fully suppress YAP in response to actin cytoskeletal changes. EMBO J. 2013; 32:1543–1555. [PubMed: 23644383]
28. Yu FX, et al. Protein kinase A activates the Hippo pathway to modulate cell proliferation and differentiation. Gene Dev. 2013; 27:1223–1232. [PubMed: 23752589]
29. Niewiadomski P, et al. Gli protein activity is controlled by multisite phosphorylation in vertebrate Hedgehog signaling. Cell reports. 2014; 6:168–181. [PubMed: 24373970]
30. Mo JS, Park HW, Guan KL. The Hippo signaling pathway in stem cell biology and cancer. EMBO reports. 2014; 15:642–656. [PubMed: 24825474]

31. Pan D. The hippo signaling pathway in development and cancer. Developmental cell. 2010; 19:491–505. [PubMed: 20951342]
32. Mohseni M, et al. A genetic screen identifies an LKB1-MARK signalling axis controlling the Hippo-YAP pathway. Nature cell biology. 2014; 16:108–117. [PubMed: 24362629]
33. Yin F, et al. Spatial organization of Hippo signaling at the plasma membrane mediated by the tumor suppressor Merlin/NF2. Cell. 2013; 154:1342–1355. [PubMed: 24012335]
34. Gunther EJ, et al. Impact of p53 loss on reversal and recurrence of conditional Wnt-induced tumorigenesis. Gene Dev. 2003; 17:488–501. [PubMed: 12600942]
35. Vitale-Cross L, Amornphimoltham P, Fisher G, Molinolo AA, Gutkind JS. Conditional expression of K-ras in an epithelial compartment that includes the stem cells is sufficient to promote squamous cell carcinogenesis. Cancer research. 2004; 64:8804–8807. [PubMed: 15604235]
36. Huelsken J, Vogel R, Erdmann B, Cotsarelis G, Birchmeier W. beta-Catenin controls hair follicle morphogenesis and stem cell differentiation in the skin. Cell. 2001; 105:533–545. [PubMed: 11371349]
37. Niemann C, Owens DM, Hulsken J, Birchmeier W, Watt FM. Expression of DeltaNLef1 in mouse epidermis results in differentiation of hair follicles into squamous epidermal cysts and formation of skin tumours. Development. 2002; 129:95–109. [PubMed: 11782404]
38. Wang LC, et al. Regular articles: conditional disruption of hedgehog signaling pathway defines its critical role in hair development and regeneration. The Journal of investigative dermatology. 2000; 114:901–908. [PubMed: 10771469]
39. Milenkovic L, Scott MP. Not lost in space: trafficking in the hedgehog signaling pathway. Science signaling. 2010; 3:pe14. [PubMed: 20388915]
40. Robbins DJ, Fei DL, Riobo NA. The Hedgehog signal transduction network. Science signaling. 2012; 5:re6. [PubMed: 23074268]
41. Regard JB, et al. Activation of Hedgehog signaling by loss of GNAS causes heterotopic ossification. Nature medicine. 2013; 19:1505–1512.
42. He X, et al. The G protein alpha subunit Galphas is a tumor suppressor in Sonic hedgehog-driven medulloblastoma. Nature medicine. 2014; 20:1035–1042.
43. Alfthan K, Heiska L, Gronholm M, Renkema GH, Carpen O. Cyclic AMP-dependent protein kinase phosphorylates merlin at serine 518 independently of p21-activated kinase and promotes merlin-ezrin heterodimerization. The Journal of biological chemistry. 2004; 279:18559–18566. [PubMed: 14981079]
44. Scoles DR. The merlin interacting proteins reveal multiple targets for NF2 therapy. Biochimica et biophysica acta. 2008; 1785:32–54. [PubMed: 17980164]
45. Laulajainen M, Muranen T, Carpen O, Gronholm M. Protein kinase A-mediated phosphorylation of the NF2 tumor suppressor protein merlin at serine 10 affects the actin cytoskeleton. Oncogene. 2008; 27:3233–3243. [PubMed: 18071304]
46. Fernandez LA, et al. YAP1 is amplified and up-regulated in hedgehog-associated medulloblastomas and mediates Sonic hedgehog-driven neural precursor proliferation. Gene Dev. 2009; 23:2729–2741. [PubMed: 19952108]
47. Huang J, Kalderon D. Coupling of Hedgehog and Hippo pathways promotes stem cell maintenance by stimulating proliferation. The Journal of cell biology. 2014; 205:325–338. [PubMed: 24798736]
48. Nishio M, et al. Cancer susceptibility and embryonic lethality in Mob1a/1b double-mutant mice. J Clin Invest. 2012; 122:4505–4518. [PubMed: 23143302]
49. Gladden AB, Hebert AM, Schneeberger EE, McClatchey AI. The NF2 tumor suppressor, Merlin, regulates epidermal development through the establishment of a junctional polarity complex. Developmental cell. 2010; 19:727–739. [PubMed: 21074722]
50. Lee JH, et al. A crucial role of WW45 in developing epithelial tissues in the mouse. EMBO J. 2008; 27:1231–1242. [PubMed: 18369314]
51. Schlegelmilch K, et al. Yap1 acts downstream of alpha-catenin to control epidermal proliferation. Cell. 2011; 144:782–795. [PubMed: 21376238]
52. Weinstein LS, et al. Activating mutations of the stimulatory G protein in the McCune-Albright syndrome. The New England journal of medicine. 1991; 325:1688–1695. [PubMed: 1944469]

53. Landis CA, et al. GTPase inhibiting mutations activate the alpha chain of Gs and stimulate adenylyl cyclase in human pituitary tumours. Nature. 1989; 340:692–696. [PubMed: 2549426]
54. Kool M, et al. Genome sequencing of SHH medulloblastoma predicts genotype-related response to smoothened inhibition. Cancer Cell. 2014; 25:393–405. [PubMed: 24651015]
55. Zhao B, et al. TEAD mediates YAP-dependent gene induction and growth control. Gene Dev. 2008; 22:1962–1971. [PubMed: 18579750]
56. Chen M, et al. Increased glucose tolerance and reduced adiposity in the absence of fasting hypoglycemia in mice with liver-specific Gs alpha deficiency. J Clin Invest. 2005; 115:3217–3227. [PubMed: 16239968]
57. Chen L, et al. Regulation of renin in mice with Cre recombinase-mediated deletion of G protein Gsalpha in juxtaglomerular cells. American journal of physiology. Renal physiology. 2007; 292:F27–37. [PubMed: 16822937]
58. Bai CB, Auerbach W, Lee JS, Stephen D, Joyner AL. Gli2, but not Gli1, is required for initial Shh signaling and ectopic activation of the Shh pathway. Development. 2002; 129:4753–4761. [PubMed: 12361967]
59. Vitale-Cross L, Amornphimoltham P, Fisher G, Molinolo AA, Gutkind JS. Conditional expression of K-ras in an epithelial compartment that includes the stem cells is sufficient to promote squamous cell carcinogenesis. Cancer research. 2004; 64:8804–8807. [PubMed: 15604235]
60. Gogos JA, Osborne J, Nemes A, Mendelsohn M, Axel R. Genetic ablation and restoration of the olfactory topographic map. Cell. 2000; 103:609–620. [PubMed: 11106731]
61. Jensen KB, Driskell RR, Watt FM. Assaying proliferation and differentiation capacity of stem cells using disaggregated adult mouse epidermis. Nature protocols. 2010; 5:898–911. [PubMed: 20431535]
62. Iglesias-Bartolome R, et al. mTOR inhibition prevents epithelial stem cell senescence and protects from radiation-induced mucositis. Cell stem cell. 2012; 11:401–414. [PubMed: 22958932]
63. Levitsky KL, Toledo-Aral JJ, Lopez-Barneo J, Villadiego J. Direct confocal acquisition of fluorescence from X-gal staining on thick tissue sections. Scientific reports. 2013; 3:2937. [PubMed: 24121824]
64. Martin D, Galisteo R, Ji Y, Montaner S, Gutkind JS. An NF-[kappa]B gene expression signature contributes to Kaposi's sarcoma virus vGPCR-induced direct and paracrine neoplasia. Oncogene. 2007; 27:1844–1852. [PubMed: 17934524]
65. Petersson M, Frances D, Niemann C. Lineage tracing of hair follicle stem cells in epidermal whole mounts. Methods in molecular biology. 2013; 989:45–60. [PubMed: 23483386]
66. Vaque JP, et al. A genome-wide RNAi screen reveals a Trio-regulated Rho GTPase circuitry transducing mitogenic signals initiated by G protein-coupled receptors. Molecular cell. 2013; 49:94–108. [PubMed: 23177739]
67. Castellone MD, Teramoto H, Williams BO, Druey KM, Gutkind JS. Prostaglandin E2 promotes colon cancer cell growth through a Gs-axin-beta-catenin signaling axis. Science. 2005; 310:1504–1510. [PubMed: 16293724]
68. Molinolo AA, et al. mTOR as a molecular target in HPV-associated oral and cervical squamous carcinomas. Clinical cancer research : an official journal of the American Association for Cancer Research. 2012; 18:2558–2568. [PubMed: 22409888]

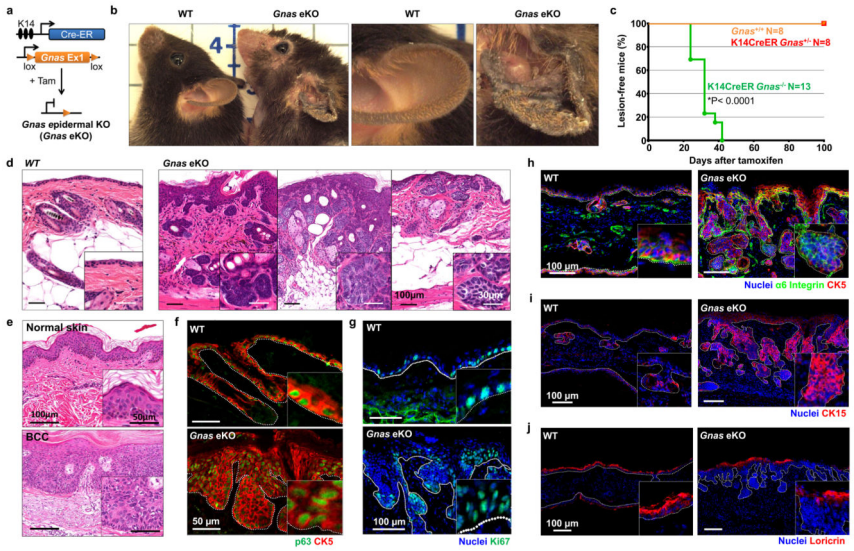

Figure 1. *Gnas* deletion from skin epidermis induces rapid basal cell carcinoma formation in mice

a, Schematic representation of the animal model used to delete *Gnas* exon 1 (Ex1) from the basal epidermal stem cell compartment. **b**, Representative pictures of WT and *Gnas* eKO animals 60 days after tamoxifen treatment. **c**, Kaplan-Meier curve of lesion-free mice. WT (*Gnas*$^{+/+}$; n=8 mice) and heterozygous *Gnas* deleted mice (K14CreER *Gnas*$^{+/-}$; n=8 mice) did not develop lesions, while homozygous deleted *Gnas* eKO mice (K14CreER *Gnas*$^{-/-}$; n=13 mice) developed lesions 20 to 40 days after tamoxifen treatment. Significance was calculated by Mantel-Cox. **d**, Histological analysis of WT and *Gnas* eKO mice. *Gnas* eKO skin shows basaloid cells growing in the stroma resembling micronodular and superficial BCC. **e**, Example of human normal and BCC skin histopathology. **f, g, h, i, j,** Representative pictures of the skin of WT and *Gnas* eKO animals stained to show expression of the stem cell marker p63 (green) and the basal progenitor marker cytokeratin 5 (CK5, red) (f); the proliferation marker Ki67 (green) and nuclei (blue) (g); CK5 (red), α6 integrin (green) and nuclei (blue) (h); the hair follicle marker cytokeratin 15 (CK15, red) and nuclei (blue) (i); and the differentiation marker loricrin (red) and nuclei (blue) (j). Insert panels in each images show details at higher magnification. Location of the basal membrane is indicated with a white dotted line.

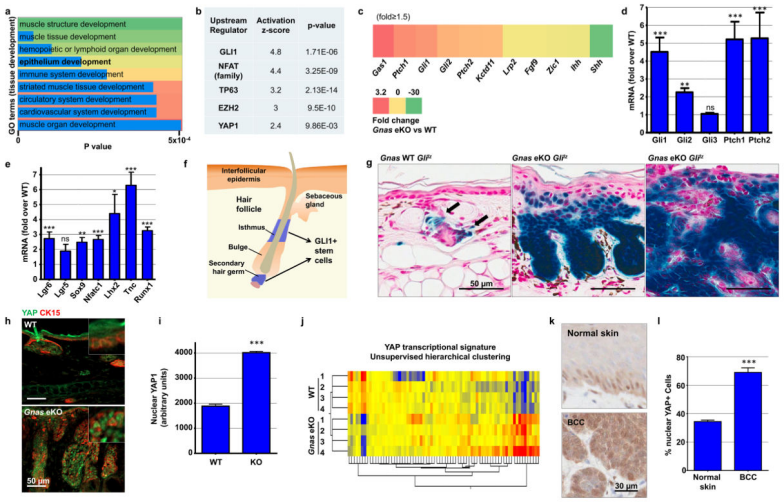

Figure 2. Genomic analysis unveils activation of GLI and YAP transcriptional networks in *Gnas* eKO mice

a, Gene ontology analysis of differentially regulated genes in *Gnas* eKO mice filtered by development terms. **b**, Functional analysis of transcriptional regulators shows epithelial stem cells factors upregulated in *Gnas* eKO mice. Generated using Ingenuity Pathway Analysis (IPA, Ingenuity® Systems) **c**, Heat map depicting the fold change of the expression level of Hedgehog signaling related genes in *Gnas* eKO vs WT mice in gene array. **d**, qRT–PCR analysis of GLI transcription factors and the GLI-regulated genes *Ptch1* and *Ptch2*. n=3 mice of each genotype (samples from 3 WT mice and 3 *Gnas* eKO mice). **e**, *Gnas* eKO mice skin qRT–PCR quantification of transcriptional regulators and markers essential for hair follicle stem cell maintenance and proliferation. n=3 mice of each genotype (samples from 3 WT mice and 3 *Gnas* eKO mice). **f**, Schematic representation of skin showing the location of the GLI positive stem cell compartment in the hair follicle isthmus and secondary hair germ. **g**, βGal staining for ear skin of WT *Gli*^{lz} and *Gnas* eKO *Gli*^{lz} mice 4 weeks following tamoxifen administration showing GLI^{+} cells. Arrows indicate the typical location of GLI^{+} stem cells. **h**, **i**, Staining (h) and quantification (i) of YAP1 expression in skin of WT and *Gnas* eKO animals. n=240 cells WT, 300 cells KO, from tissue samples from 3 WT mice and 3 *Gnas* eKO mice. **j**, Unsupervised hierarchical clustering using a YAP1 transcriptional signature in gene array analysis. **k**, **l**, Immunostaining (k) and quantification (l) of YAP1 expression in human normal skin and BCC. n= 3 normal and 6 BCC tissue sections. Data are presented as means±s.e.m., and significance was calculated by ANOVA and Student's t-test (NS $P > 0.05$; *$P < 0.05$; **$P < 0.01$; and ***$P < 0.001$).

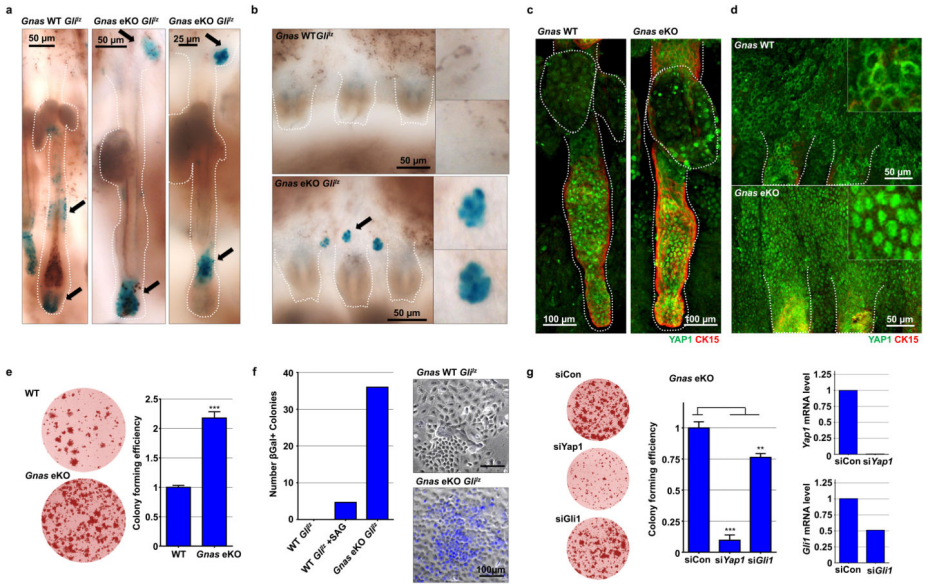

Figure 3. *Gnas* eKO triggers ectopic/de novo activation of GLI and YAP1

a, **b**, Representative pictures of βGal staining of tail skin whole mounts from WT *Gli*^{lz} and *Gnas* eKO *Gli*^{lz} mice showing GLI^{+} cells one day after finishing the administration of tamoxifen. Arrows indicate the location of GLI^{+} epithelial stem cells. In b hair follicles were removed to facilitate visualization of GLI activation at the base of the isthmus of hair follicles. **c, d,** Representative pictures of tail skin whole mounts from WT and *Gnas* eKO animals stained to show expression of YAP1 (green) and cytokeratin 15 (CK15, red), one day after finishing the administration of tamoxifen. **e**, Representative pictures of wells and quantification of clonogenic assays of keratinocytes isolated from WT and *Gnas* eKO mice two weeks after tamoxifen treatment. n=3 technical replicates, one representative experiment of three is shown. **f**, Quantification and representative pictures of βGal positive keratinocyte colonies from WT *Gli*^{lz} and *Gnas* eKO *Gli*^{lz} mice. Cells from 2 mice of each genotype were plated in duplicate and colonies counted (cells from 2 WT mice and 2 *Gnas* eKO mice). **g**, Representative pictures of wells and quantification from clonogenic assays of keratinocytes isolated from *Gnas* eKO mice and transfected with the corresponding siRNAs. Graphs on the right show mRNA levels of *Gli1* and *Yap1* after transfection with respective siRNAs. n=3 technical replicates, one representative experiment of three is shown. Insert panels in images show details at higher magnification. Hair follicles are delineated with a white dotted line.

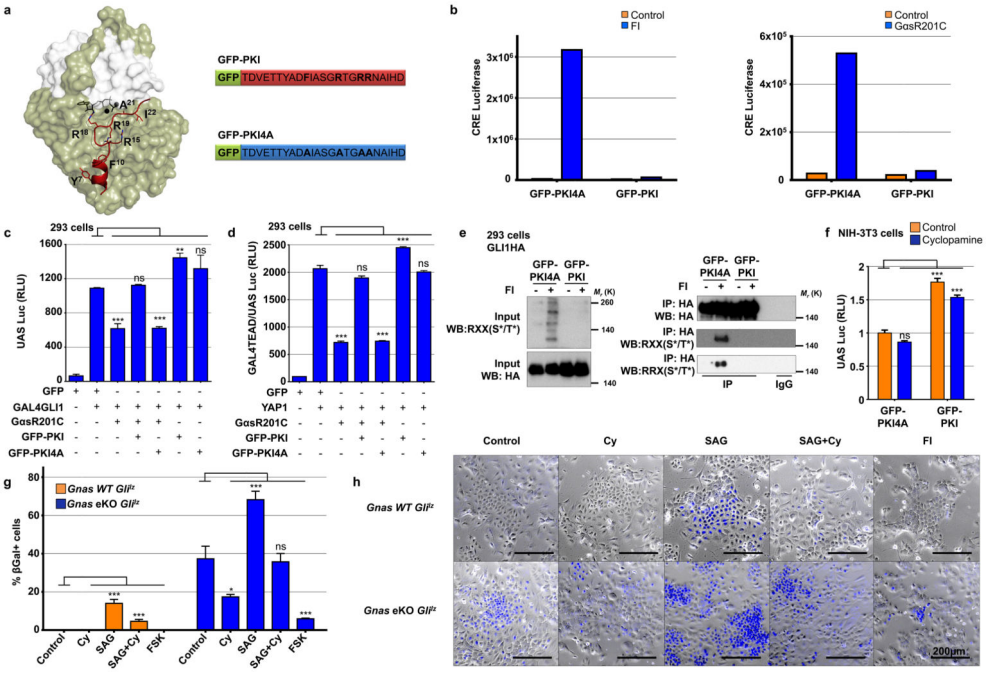

Figure 4. Gαs-PKA restrain GLI and YAP1 transcriptional activity

a, Structure of PKA bound to the active PKA inhibitor protein (PKI) peptide and amino-acid sequence of PKI and its inactive mutant PKI4A. **b**, Both forskolin and the Gαs active mutant GαsR201C are able to activate a CRE luciferase reporter in 293 cells expressing the inactive GFP-PKI4A mutant, while GFP-PKI completely blocks this response. Data from one representative experiment of three are shown. **c, d**, Transcriptional activity measured by luciferase assay of GLI1 (d) and YAP1 (e) in 293 cells transfected with the indicated DNAs. GLI1 activity was measured by GAL4GLI1/UASLuc and YAP1 by GAL4TEAD/UASLuc reporters. The constitutive active mutant GαsR201C was used to mimic Gαs activation and PKI was used to block PKA activity (see also Supplementary Fig. 3). n=3 independent experiments. **e**, Phosphorylation of GLI1 by PKA. 293 cells were transfected with the indicated DNAs and GLI1-HA. Then, cells were treated with forskolin (FSK) for 30 min and GLI1-HA was immunoprecipitated and tested with two different anti-phospho-PKA substrate motif antibodies that detect proteins containing phospho-serine/threonine residues with arginine at the −3 and −2 positions [RXX(S*/T*) and RRX(S*/T*)]. Full images of blots are shown in Supplementary Fig. 6. **f**, Transcriptional activity of GLI1 in NIH3T3 cells measured by GAL4GLI1/UASLuc reporters co-transfected with the indicated DNAs and treated or not with cyclopamine. n=3 independent experiments. **g**, **h**, Quantification (h) and representative pictures (i) of βGal staining of keratinocytes from WT *Gli*^{lz} and *Gnas* eKO *Gli*^{lz} mice treated with the indicated drugs for 48hs. Cells isolated from WT or *Gnas* eKO mice were plated in triplicate, treated and positive and negative cells were counted (between 1000 and 1500 cells per condition were counted). One representative experiment of three is shown. RLU: relative luciferase units; Cy: cyclopamine; FI: forskolin+IBMX. Data are presented as means±s.e.m., and significance was calculated by ANOVA and Student's t-test (NS $P > 0.05$; *$P < 0.05$; **$P < 0.01$; and ***$P < 0.001$).

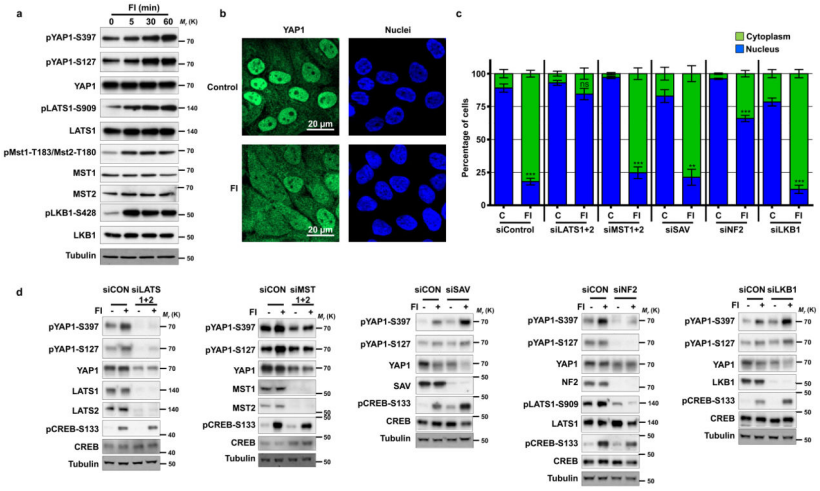

Figure 5. PKA mediates cAMP-induced inactivation of YAP1 through LATS and NF2

a, Western blot analysis of YAP1 regulatory molecules in non-confluent HACAT cells treated with with cAMP raising agents, forskolin+IBMX (FI), for the indicated times. **b**, Representative pictures of non-confluent HACAT cells treated or not with forskolin+IBMX (FI) for 2 hs and stained to show expression of YAP1 (green) and nuclei (blue). **c**, **d**, RNA interference experiments of the indicated YAP1 regulatory molecules. Cells were transfected with indicated siRNAs for 48hs and then treated (FI) or not (C) with forskolin+IBMX for 2 hs and stained to show expression of YAP1 (c); or harvested for the indicated Western blot analysis (d). For d, the proportion of cells per field showing YAP1 localization in the nucleus or cytoplasm was quantified. n=3 independent experiments, 4 fields with 30 to 50 cells were counted per condition per experiment. Data are presented as means±s.e.m., and significance was calculated in the nucleus fraction by Student's t-test against the control of the same group (NS $P > 0.05$; *$P < 0.05$; **$P < 0.01$; and ***$P < 0.001$). Full images of blots are shown in Supplementary Fig. 6.

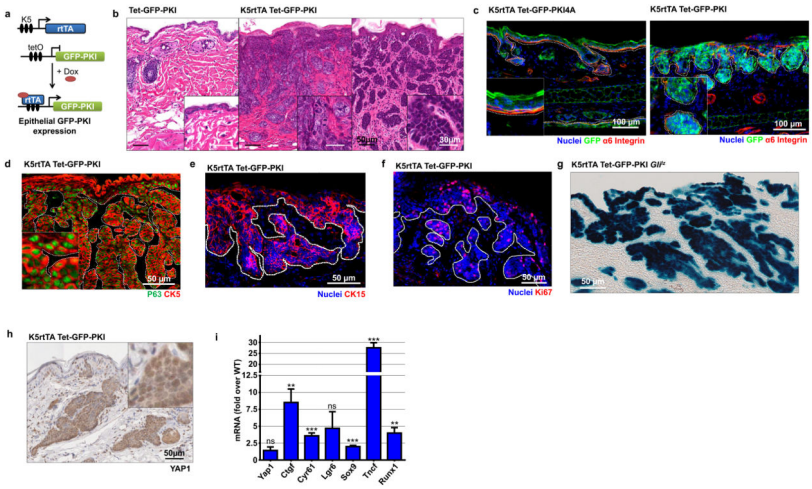

Figure 6. Inactivation of PKA is sufficient to initiate basal cell carcinoma formation

a, Schematic representation of the animal model used to target the inducible expression of the PKA inhibitor protein (GFP-PKI) to the basal epidermal stem cell compartment. **b**, Histological analysis of WT and K5rtTA Tet-GFP-PKI mice. K5rtTA Tet-GFP-PKI skin shows basaloid cells growing in the stroma resembling micronodular and superficial BCCs. **c,** Representative pictures of the skin of K5rtTA Tet-GFP-PKI4A and K5rtTA Tet-GFP-PKI mice stained to show expression of GFP (green), α6 integrin (red) and nuclei (blue). **d, e, f,** Representative pictures of the skin of K5rtTA Tet-GFP-PKI animals stained to show expression of the stem cell marker p63 (green) and the basal progenitor marker cytokeratin 5 (CK5, red) (d); the hair follicle marker cytokeratin 15 (CK15, red) and nuclei (blue) (e), and the proliferation marker Ki67 (red) and nuclei (blue) (f). **g**, Representative picture of βGal staining of the skin of K5rtTA tet-GFP-PKI *Gli*^{lz} mice showing activation of GLI. **h**, Representative picture of YAP1 immunohistochemistry staining of the skin of K5rtTA tet-GFP-PKI showing nuclear localization of YAP1 in skin lesions. **i**, qRT–PCR analysis of mRNA levels of *Yap1* and the YAP1-regulated gene *Ctgf*, and transcriptional regulators and markers essential for hair follicle stem cell maintenance and proliferation in primary cultures of keratinocytes from K5rtTA tet-GFP-PKI mice compared to cultures from WT littermates. n=3 independent cultures from 3 WT and 3 K5rtTA tet-GFP-PKI mice. Data are presented as means±s.e.m., and significance was calculated by ANOVA and Student's t-test (NS $P > 0.05$; *$P < 0.05$; **$P < 0.01$; and ***$P < 0.001$). Insert panels in images show details at higher magnification. Location of the basal membrane is indicated with a white dotted line.

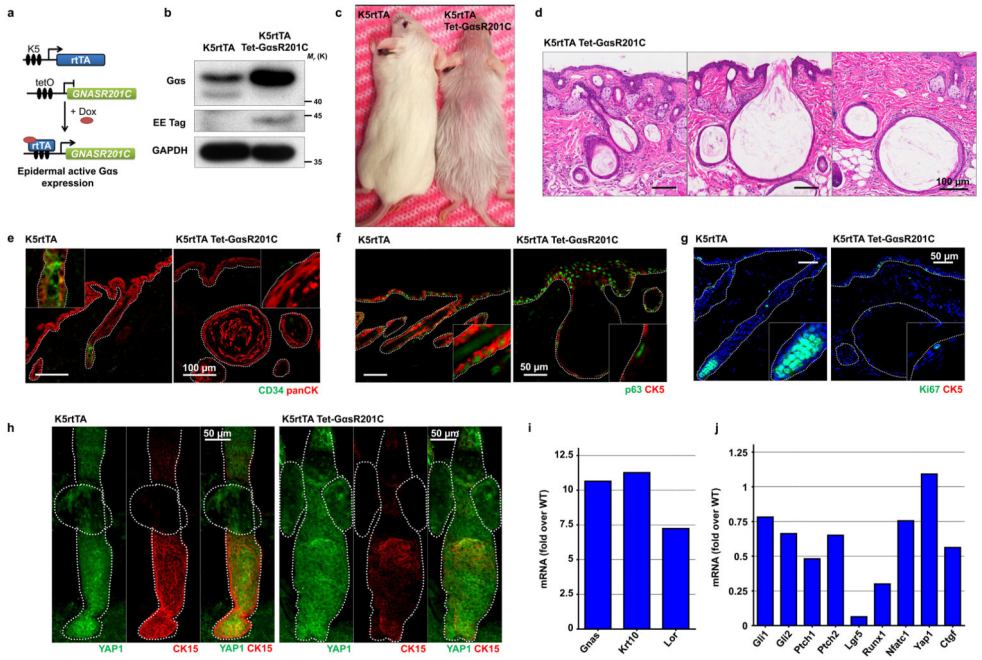

Figure 7. Gαs activation in the skin leads to epidermal stem cell differentiation and premature hair loss

a, Schematic representation of the animal model. **b**, Western blot analysis of keratinocytes isolated from control (K5rtTA) and active Gαs mice (K5rtTA tet-GαsR201C) treated with doxycycline (to induce transgene expression). Full images shown in Supplementary Fig. 6. **c**, Representative picture of control and active Gαs mice 5 months after doxycycline treatment. **d**, Histological analysis of skin from active Gαs mice showing hair follicles differentiated into keratinized cysts structures. **e, f, g**, representative pictures of skin stained to show expression of the hair follicle stem cell marker CD34 (green) and pan-cytokeratin (panCK, red) (e); the stem cell marker p63 (green) and the basal progenitor marker CK5 (red) (f); and the proliferation marker Ki67 (green) and nuclei (blue) (g). Insert panels in images show details at higher magnification. Location of the basal membrane is indicated with a white dotted line. **h**, Representative pictures of hair follicles from tail skin whole mounts in mice treated with doxycycline for 2 months. Staining shows YAP1 (green) and cytokeratin 15 (CK15, red). Details at higher magnification can be seen in Supplementary Fig. 5. Hair follicles are delineated with a white dotted line. **i, j**, qRT–PCR analysis of the expression of *Gnas* and the differentiation markers cytokeratin 10 (*Krt10*) and loricrin (*Lor*) (j), *Gli* transcription factors (k), GLI-regulated genes *Ptch1* and *Ptch2* (k), hair follicle stem cell markers (*Lgr5*, *Runx1*, *Nfatc1*) (k), *Yap1* and the YAP1-regulated gene *Ctgf* (k), in primary culture of keratinocytes. Data from one representative experiment of three are shown. Data are presented as means.

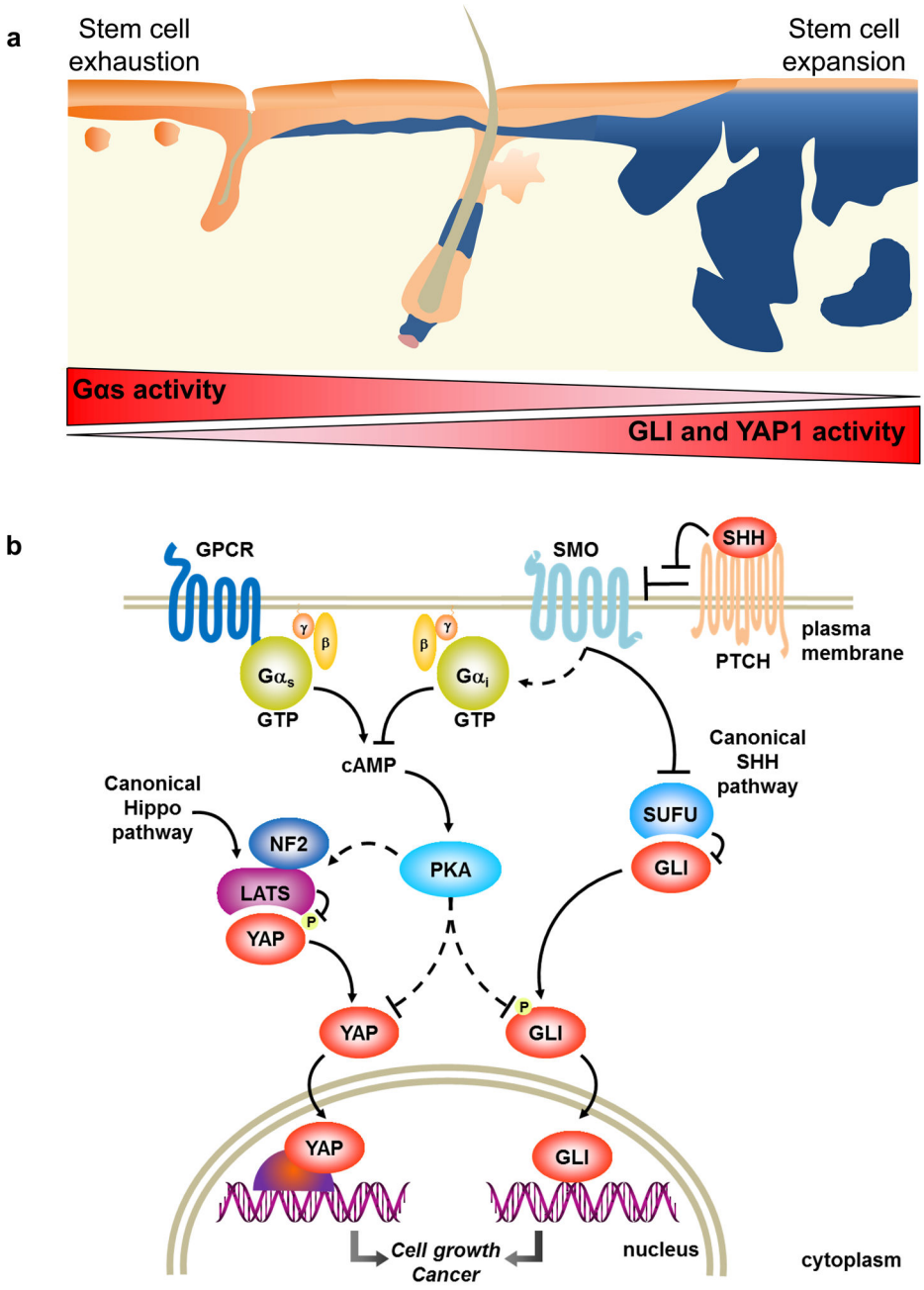

Figure 8. Model of the regulation of stem cell fate in the epidermis by Gαs-PKA

a, b, In contrast with the well-known tumor promoting role of the heterotrimeric G protein Gαs, this study suggests that Gαs and its downstream effector PKA function as part of a tumor suppressive circuitry regulating the fate of GLI^{+} stem cells (shown in blue in a), in part by restraining the transcriptional activity YAP1 and GLI, independently of canonical Hippo and SHH signaling (b). Disruption of this Gαs-PKA signaling axis in the epidermis is sufficient to promote rapid stem cell expansion and basal cell carcinoma formation, while

overactivation of this signaling pathway leads to hair follicle stem cell depletion and hair loss (a). See text for more details.